Active Probes for Network Analysis within 70–230 GHz

Oliver Wohlgemuth, Mark J. W. Rodwell, *Member, IEEE,* Ralf Reuter, Jürgen Braunstein, and Michael Schlechtweg, *Member, IEEE*

Abstract— **This paper presents a vector network analyzer system for the 70–230-GHz bandwidth. The instrument employs active probes for millimeter-wave signal generation and detection, and for signal delivery to the device-under-test. Milimeter-wave signals are generated and detected within the active probes using an integrated circuit (IC) based on nonlinear transmission lines. The IC contains all elements of an S-parameter test set: a multiplier to generate the radio-frequency signal, directional couplers to separate the incident and reflected waves, and a pair of high-speed sampling circuits to convert the signals down to lower frequencies. Two-port measurements over the 70–230-GHz bandwidth are demonstrated, including those of directional couplers and millimeter-wave high electron-mobility transistors.**

Index Terms— **Active probes, network analyzer, nonlinear transmission line, sampling circuit, S-parameter measurement system.**

I. Introduction

RECENT advancement of III–V devices, especially with InP-based devices has led to transistors with very high-power gain cutoff $f_{\max}$. Both high electron-mobility transistors (HEMT's) [1] and heterojunction bipolar transistors (HBT's) [2] have attained $f_{\max}$ greater than 500 GHz. Using such high-speed transistors, integrated circuits (IC's) operating above 120 GHz have been demonstrated [3], [4]. Commercial broad-band on-wafer S-parameter measurement setups are currently limited to a 120-GHz bandwidth. Design of monolithic microwave integrated circuits (MIMIC's) for 120-GHz operation thus requires transistor characterization and model extraction over the dc–120-GHz bandwidth, followed by use of this (extrapolated) model over an extended frequency range. Particularly for more complex circuits, such extrapolated models do not have sufficient accuracy. IC design in the 140–220-GHz band demands a measurement system for device characterization above 120 GHz.

In this paper, we report a network analysis system for on-waver S-parameter measurements over the 70–230-GHz bandwidth. The instrument consists of active probes, containing millimeter-wave S-parameter test sets in the form of GaAs millimeter-wave IC's. Within these IC's, GaAs nonlinear transmission lines are used for stimulus signal frequency multiplication, monolithic directional couplers are used for independent measurement of incident and reflected waves, and nonlinear transmission line (NLTL)-gated sampling circuits serve as harmonic mixers for frequency down-conversion of the measured incident and reflected waves. The active probes interface to the IF signal of an HP8510 network analyzer, and serve to extend its frequency range. The use of the HP8510 allows relatively easy and fast S-parameter measurements.

An active probe-based network analyzer (NWA) using GaAs NLTL IC's had earlier been reported by Yu *et al.* [5]. Among improvements over that work, the present IC uses true directional couplers for high directivity and low-order harmonic generation in the stimulus signal generation. In addition the detected (IF) signals are processed in the frequency domain, without using time-domain/Fourier transform methods. A high-pass filter at the output of the source frequency multiplier equalizes its output power spectrum, further increasing the signal-to-noise ratio at high frequencies. By packaging the chips into active probes and incorporating buffer amplifiers close to the chip, the IF can be increased to 20 MHz, which decreases the phase noise and allows the HP8510 to be used directly for IF signal processing. Together, these improvements substantially increase the system signal-to-noise ratio and directivity.

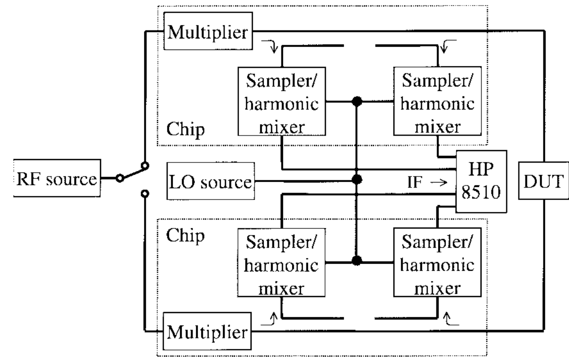

Fig. 1. Typical S-parameter measurement setup.

II. Monolithic S-Parameter Test Set

Fig. 1 shows a typical S-parameter measurement system. An RF source drives a frequency multiplier that generates the high-frequency signal. Two directional couplers are used to

Manuscript received March 26, 1999; revised July 9, 1999. This work was supported by the German Ministry of Education and Research.

O. Wohlgemuth, R. Reuter, J. Braunstein, and M. Schlechtweg are with the Fraunhofer Institute for Applied Solid State Physics, D-79108 Freiburg, Germany.

M. J. W. Rodwell is with the Department of Electrical and Computer Engineering, University of California at Santa Barbara, Santa Barbara, CA 93106 USA.

Publisher Item Identifier S 0018-9480(99)08460-4.

0018–9480/99$10.00 © 1999 IEEE

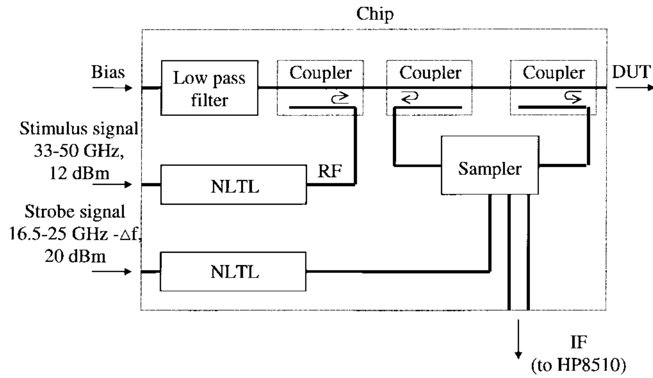

Fig. 2. Block diagram of the S-parameter test-set IC.

separate the incident and reflected signals. Harmonic mixers or samplers are used to convert the signals to a lower (intermediate) frequency. These mixers are driven from the LO source. The amplitudes and phase of the IF signals are then measured and evaluated by the HP8510. At higher frequencies, reflections at discontinuities become severe and the loss of cables or waveguides becomes greater, resulting in a poorer directivity at higher frequencies. The objective of this study was to integrate all high-frequency components of the S-parameter test set on a single IC [6] so that cables, waveguides, and connections are not present in the 70–230-GHz signal path. For the 70–230-GHz signal, only the connection to the device-under-test (DUT) is necessary, which can be very short by packaging the chips into active probes [7], [8]. Use of NLTL's within the monolithic S-parameter test set allows frequency multiplication in a very wide bandwidth [9]. In addition NLTL's can drive the LO ports of millimeter-wave diode sampling circuits to convert the RF signals down to the IF bandwidth used by the HP8510.

Fig. 2 shows a block diagram of the monolithic S-parameter test set. The stimulus source drives an NLTL, which is used as a frequency multiplier. The NLTL drives the test port through a directional coupler. The coupler functions as a bias tee, isolating the NLTL frequency multiplier from the dc bias applied to the test port. Further, the coupling increases with frequency, thereby reducing the variation of the DUT drive power with frequency. Two additional couplers are integrated to separate the incident and reflected waves and two high-speed sampling circuits are used to convert the signals down to 20-MHz intermediate frequency. The LO ports of the sampling circuits are driven by a second NLTL pulse generator. To reduce reflections from the dc bias connection to the active probe, a low-pass filter is also integrated on the IC. Originally, the multiplier NLTL was designed for a drive frequency from 33 to 50 GHz, and the strobe NLTL for a drive frequency from 16.5 to 25 GHz, thus, the third and fourth harmonic of the RF and the sixth and eighth harmonic of the LO cover a 100–200-GHz bandwidth. However, with increasing the drive powers at lower frequencies, NLTL pulse compression is increased, and generation of higher order harmonics enhanced. The instrument bandwidth could thus be increased. Using the fifth harmonic of the RF signal and the eighth harmonic of the LO signal, the instrument operates over the 70–230-GHz bandwidth.

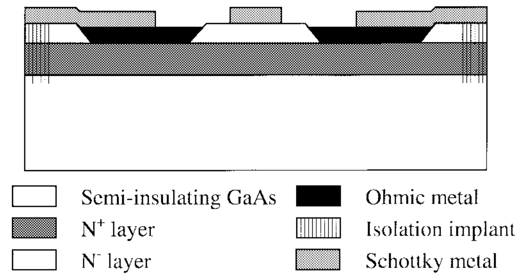

Fig. 3. Cross section of a Schottky varactor diode.

III. Nonlinear Transmission Line

An NLTL [9], [10] is a transmission line with relatively high impedance, periodically loaded with reverse-biased Schottky varactor diodes. This forms a synthetic transmission line, whose propagation velocity is voltage dependent, so that different portions of a wave propagate with different velocities. For a negative-going wave transition, the initial parts of the transition, near 0 V, propagate more slowly than the final part of the transition. Propagating along the line, the fall time becomes shorter. As the fall time decreases, dispersion arising form the periodic-line cutoff frequency (Bragg frequency) and the varactor diode cutoff frequency competes with the compression arising from the voltage-dependent propagation velocity. The final limited fall time is reached when the compression per section is balanced with the fall time broadening per section arising from the Bragg frequency and the cutoff frequency of the diodes. With a sinusoidal input signal, the NLTL forms a shock-wave from the negative-going half-cycles of the sinusoid, producing a saw-tooth output waveform with significant power level at high-order harmonics of the signal frequency.

IV. Technology

The NWA circuit is implemented in a seven-mask process. On a semiinsulating GaAs wafer, a highly doped N^+ layer ($7 \cdot 10^{18}$ cm^{-3}) is grown by molecular beam epitaxy. For the active layer of the Schottky diodes, an N^- layer, with an exponential doping profile, is then grown [10], [11]. The exponential doping profile combines a large capacitance variation and a high breakdown voltage (13 V) with a high diode large-signal cutoff frequency (2.5 THz). Fig. 3 shows a diode cross section. Ohmic contacts to the N^+ layer are formed by a recess etch through the N^- layer, followed by a self-aligned AuGe–Ni–Au liftoff and a subsequent rapid thermal annealing. This produces contacts, with a resistance of 25 $\Omega \cdot \mu$m. The N^+ layer sheet resistance is 7.5 Ω per square. The diode junction areas and resistors are defined by proton implantation, which converts the implanted semiconductor into an insulator. For the Schottky contacts, Ti/Pt/Au is deposited and where this overlays unimplanted areas, a Schottky contact is formed. Very small diodes, with 1-μm feature size, are required in the sampling circuits. With such small feature sizes, the deposited Schottky contact metal must be relatively thin. Thus, the interconnect metal of 1.4-μm thickness for reduced microwave loss is deposited in the next process step. To provide capacitors, a 2500 Å Si_3N_4 film is then deposited by

PECVD. Air bridges, for signal line crossovers and capacitor top plates, are then formed by electroplating, completing the process.

V. Design and Results

A. Source Frequency Multiplier

The DUT stimulus signal source is generated by an NLTL operating as a millimeter-wave frequency multiplier. Unlike [5], low-order frequency multiplication is employed, increasing the multiplier conversion efficiency. This requires a high NLTL drive frequency, 50 GHz for a 200-GHz output if 4:1 frequency multiplication is used. Unless specific design measures are taken, high drive frequencies result in increased skin-effect losses on the NLTL, seriously degrading NLTL frequency multiplier performance. On the NLTL, the strongest diode capacitance variation is for signals near 0 V. Propagating along the line, the signal amplitude is attenuated, and the peak positive signal excursion may not approach 0 V near the NLTL output. The diodes near the NLTL output are driven only through a small capacitance variation, resulting in reduced compression and reduced harmonic generation. With reduced compression, the NLTL length must be increased, further compounding skin-effect losses.

Therefore, skin-effect losses must be minimized by special design strategies. The NLTL is divided into two parts: a first section using normal coplanar waveguide (CPW) and a second section using elevated coplanar waveguide. In the first section, the Bragg frequency is tapered with propagation distance. Near the input of the first section, the Bragg frequency is low, resulting in long diode–diode separations. The lateral dimensions of the CPW can, thus, also be large, resulting in large conductor widths and low skin-effect losses. As the signal propagates along the line, the signal bandwidth increases, and the Bragg frequency must be proportionally increased to permit propagation of the generated harmonics. At all points along the line, the Bragg frequency is set no higher than required for the local signal bandwidth, locally maximizing the conductor width and minimizing the conductor losses.

Thus, CPW lateral dimensions progressively decrease along the NLTL length. Once the lateral (ground–ground) CPW dimensions have been reduced to $\approx$60 μm, CPW skin-effect losses can be substantially reduced by using air-bridge processes to elevate the CPW signal conductor 2–3 μm above the substrate. The second NLTL section uses such elevated CPW [12]. With the center conductor in the air, the effective dielectric constant is reduced, and a wider conductor must be used for a given CPW impedance. The wider CPW center conductor results in reduced skin-effect losses. This is of particular importance near the output end of the NLTL, where the Bragg frequency is high and the overall conductor dimensions small.

Additionally, skin-effect losses are compensated by changing the loaded large-signal impedance from 40 to 50 Ω by the second part of the NLTL [8]. The increased loaded characteristic impedance increases the signal voltage swing, offsetting the effects of attenuation. This ensures that the diodes near the NLTL output are driven through a large voltage swing, maintaining strong compression (and strong harmonic generation) for the output sections of the NLTL. Fig. 4 shows the measured output waveform of this NLTL with a fall time of 3.2 ps. The observed 3.2 ps includes the effects of the sampling circuit bandwidth, hence, the true NLTL transition time is somewhat smaller.

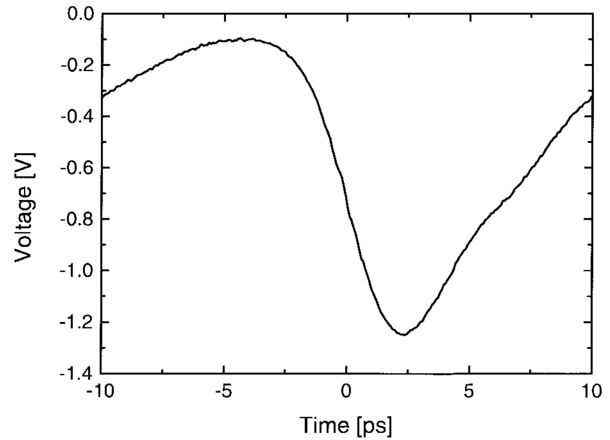

Fig. 4. Output voltage waveform of the multiplier NLTL with a fall time of ~3.2 ps.

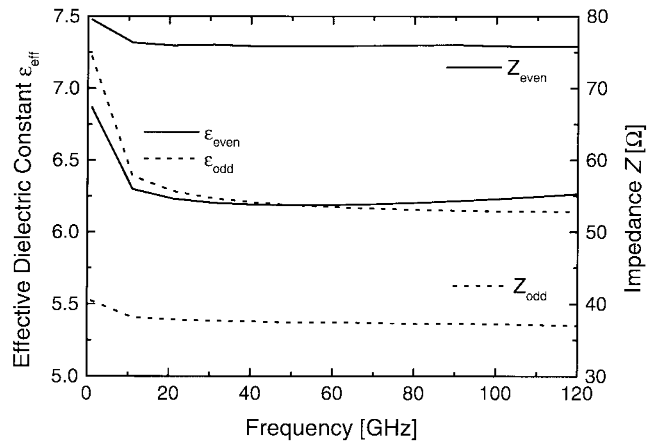

Fig. 5. The effective dielectric constants and the impedances of the even and odd modes of the coplanar directional coupler.

B. Directional Coupler

To design the coplanar directional couplers, the impedances $Z_{\rm even}$ and $Z_{\rm odd}$ and the complex propagation constants $\gamma_{\rm even}$ and $\gamma_{\rm odd}$ were first calculated using a three-dimensional (3-D) simulator.[1] Fig. 5 shows the impedances and (from $\gamma_{\rm even}$ and $\gamma_{\rm odd}$) the calculated effective dielectric constants of the even and odd modes for a 10-dB coupler. The data of Fig. 5 present clear advantages of coplanar directional couplers over microstrip couplers: the effective dielectric constants of the even and odd modes are nearly equal and the mode impedances are almost independent of frequency. This is important for high directivity broad-band line couplers [13], [14].

[1] HP 85180A, High-Frequency Strucutre Simulator (HFSS), Hewlett-Packard Company, Santa Rosa, CA.

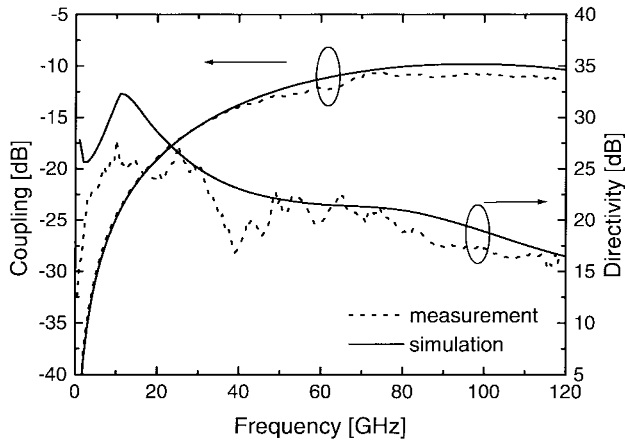

Fig. 6. Simulated and measured coupling and directivity of the coupler, designed for 90-GHz center frequency.

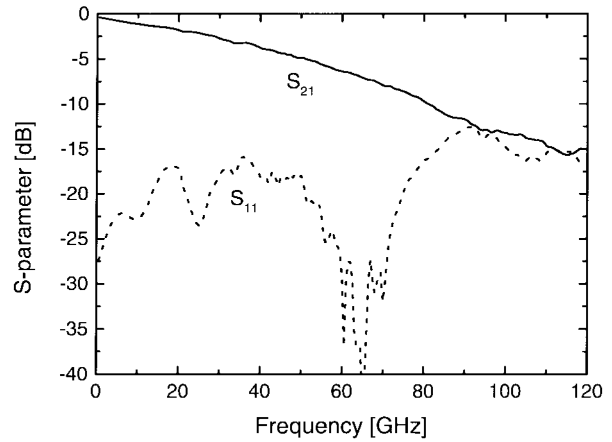

Fig. 8. Attenuation and reflection of the low-pass dc-bias isolation filter.

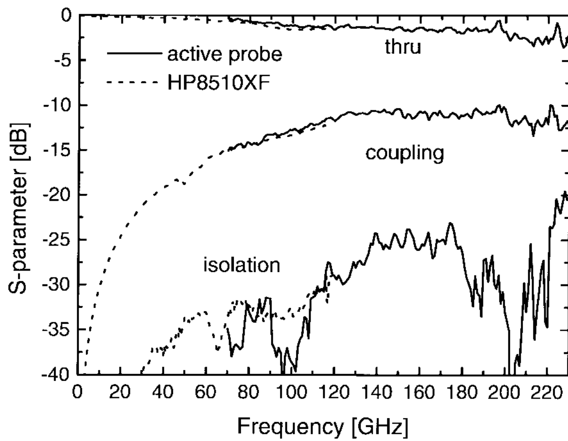

Fig. 7. S-parameter measurement of a coplanar directional 10-dB coupler, designed for 180-GHz center frequency.

To verify the simulation, one coupler was scaled in length for a center frequency of 90 GHz, fabricated, and measured in W-band. Fig. 6 shows the directivity and coupling, comparing simulation to measurement. The couplers used in the S-parameter test-set IC were scaled in length to obtain a 180-GHz center frequency. Such couplers were also fabricated as isolated test structures, and tested with the active probe system itself (Fig. 7).

C. Low-Pass Filter

To test active devices, the active probes must provide dc-bias connections for the DUT. If there are high reflections (arising from bond wires and from microwave connectors) at the dc-bias connection to the test-set IC, the reflected wave may interfere with the stimulus signal, resulting in poor instrument directivity. Over the 70–230-GHz instrument bandwidth, the DUT dc-bias connections to the S-parameter test-set IC are isolated from the DUT test port by a low-pass filter. The low-pass filter must itself have a low output reflection coefficient.

The bias port low-pass filter is implemented as a lossy synthetic 50-Ω transmission line. The one-pass attenuation of the filter can be moderate because waves, reflected from the bias connection, must pass twice through the filter to return to the DUT. Using a external 50-Ω bias tee and short bond wires, the reflection at the dc-bias connection to the IC will be small over a dc–50-GHz bandwidth. The filter can thus be designed to pass signals below $\approx$50 GHz, and to have $>$7-dB attenuation above 70 GHz. This will ensure $>$14-dB return loss at the DUT port over the 70–230-GHz instrument bandwidth.

The filter is implemented as a high-impedance CPW loaded by Si_3N_4 capacitors to form a synthetic 50-Ω transmission line. To provide the required range of dc-bias currents, the CPW center conductor must be relatively wide. Consequently, CPW skin-effect losses are too low to provide effective isolation. Instead, small resistances R placed in series with each of the N loading capacitors C introduce frequency-dependent attenuation $\alpha \approx N\omega^2 C^2 R Z_o/2$. These resistors have no effect on the dc bias applied to the line. As a synthetic transmission line, the bias filter design is similar to the design of an NLTL. The filter Bragg frequency must be higher than 230 GHz to avoid reflection due to the filter high-frequency cutoff. Elevated CPW is used because this combines a high Bragg frequency with a wide center conductor, which can carry a high dc current. Without capacitive loading, the elevated CPW has 75-Ω impedance, and is reduced to 50-Ω by the loading capacitors. The resistive loading is nonuniform. Near the DUT, the resistive loading is small, as the loading perturbs the loaded characteristic impedance and, hence, the output return loss. Nearer the bias port connection, the loading is higher, to ensure a high net attenuation. Fig. 8 shows the S-parameter measurement of the low-pass filter with the bias line. The one-pass transmission is about 7 dB at 70 GHz, thus, a signal reflected from the bias connection is at least attenuated by 14 dB. The output reflection coefficient of the low-pass filter is better than 13 dB.

D. Sampling Circuits

The sampling circuits consists of a balun/differentiator and a diode/resistor bridge, and the schematics are shown in Fig. 9 [15]–[17]. A picosecond-fall-time step function, produced from the NLTL, is coupled through the matching network into the coplanar strip (CPS) mode of the lines, which carry the signals to be measured in the CPW mode. The air

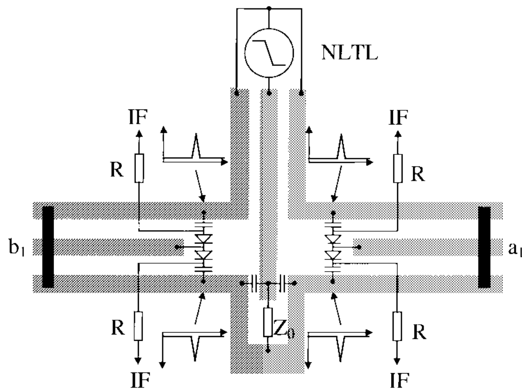

Fig. 9. Sketch of physical layout of the sampling circuits.

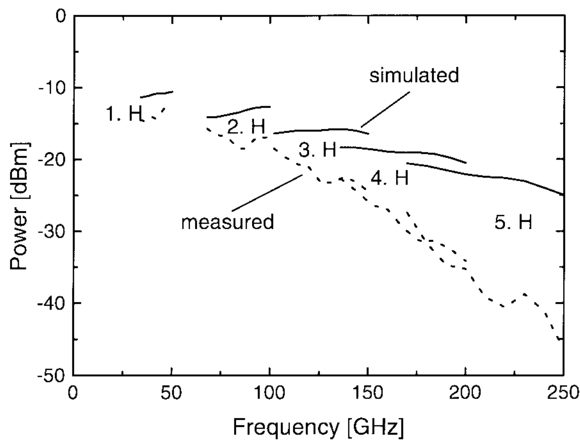

Fig. 10. Simulated and measured power at the DUT. The measurement is not corrected for the sampling circuit attenuation.

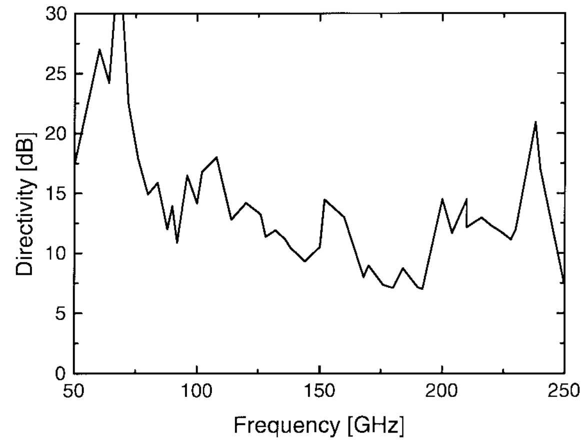

Fig. 11. Measured directivity of the full S-parameter test-set IC.

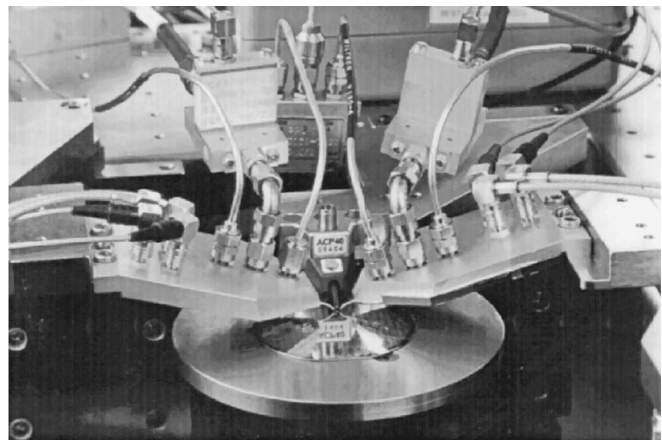

Fig. 12. The active probes mounted on a wafer probe station. The commercial probe in the background provides a scale comparison.

bridge at the distance $d_{\rm short}$ short circuits the CPS mode and reflects the step function. At the sampling diodes balanced impulses of the duration $2d_{\rm short}/v_{\rm CPS}$ are thus generated. These complementary impulses drive the sampling diodes into forward conduction and the sampling capacitors are partly charged in proportion to the signal voltage of the CPW mode. If the RF frequency is $f_{\rm RF} + \Delta f$ and the LO frequency is $f_{\rm RF}/n$, the IF frequency, developed at the hold capacitors, is Δf (where n is harmonic order used in the sampling circuit). The sampled IF voltages, isolated through the resistors R from the sampling bridge, are applied to high-impedance input buffer amplifiers.

E. Results of the Full Chip

Prior to active probe assembly, two measurements were performed to characterize the test-set IC: the power at the test port and the directivity of the full chip. To measure the power at the test port, one NWA circuit is connected to an on-wafer sampling circuit. Fig. 10 shows the measured test-port power, with the multiplier NLTL driven by 12-dBm input power. The output power varies from −14 to −35 dBm over the 50–200-GHz bandwidth, 5–15 dB lower than simulated. The discrepancy lies in the frequency-dependent attenuation of the sampling circuits, which is approximately 1 dB at lower frequencies and increases up to an estimated 10 dB at 200 GHz. Additional causes of the discrepancy between measurement and simulation include the skin-effect losses of the couplers (which could not be simulated) and additional CPW skin-effect losses arising from the high-resistivity Ti/Pt adhesion layer under the CPW transmission lines. At 200 GHz, the stimulus signal power is more than −35 dBm, which is sufficient for a high signal-to-noise ratio at the IF ports. The stimulus power of −14 dBm at lower frequencies can be too high for testing high-gain amplifiers under small-signal linear conditions, thus, a second IC was fabricated with an additional coupler in the stimulus signal path to attenuate the drive power at lower frequencies. The power at the DUT for this circuit is below −25 dBm for all frequencies.

To measure the directivity of the full IC, the incident and reflected waves of an NWA circuit with the open test port are compared with the measurement of a second NWA circuit with a nominal 50-Ω (44±1.5 Ω) chip resistor (Fig. 11). The directivity is >10 dB, dropping to ∼7 dB in a band between 160–190 GHz.

VI. The Active Probe

The NWA chips are packaged into active probes, thus, only a short transmission-line connection to the DUT is needed. Fig. 12 shows the active probes mounted on a wafer probe station in comparison to a commercial probe, and Fig. 13 shows the bottom view of a probe. The chip is mounted next

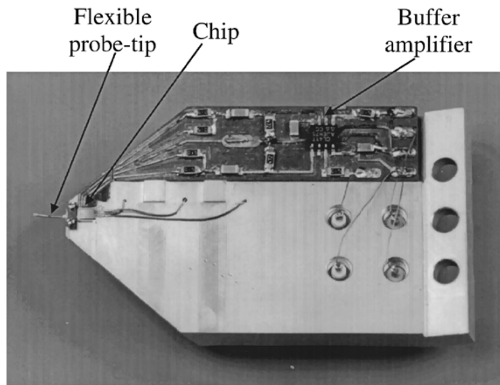

Fig. 13. Bottom view of the active probe.

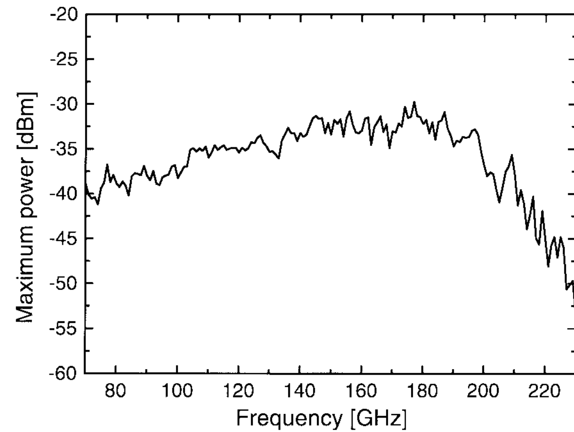

Fig. 15. Measured maximum power at the IF ports.

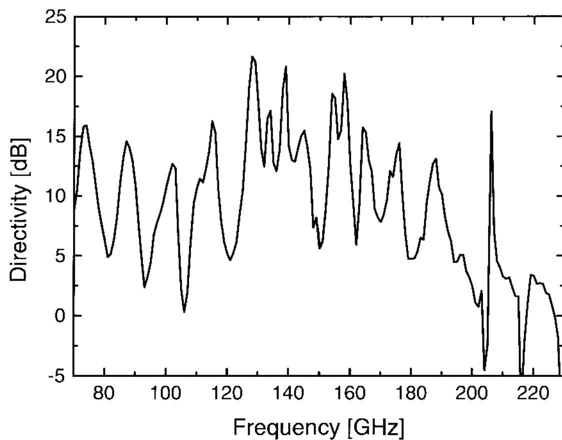

Fig. 14. Measured directivity of the active probe.

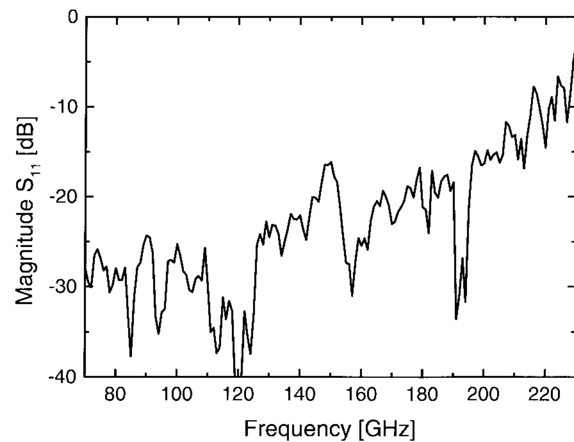

Fig. 16. Measured S_{11} of a 900-μm-long line.

to the probe tip. The connection to the DUT is provided by a flexible micro-coax cable. These coaxial probe tips were obtained from commercial (GGB Industries, Naples, FL) microwave wafer probes. The connections between the chip and the probe's V- and K-connectors are also made with micro-coaxial cable. This avoids crosstalk between the RF signal and LO signal lines, which arose in earlier packaging efforts, in which the signals were routed on transmission lines on a quartz substrate.

The high-speed sampling circuits have a very high output resistance. If the IF cables were directly connected to the sampling circuits, the cable capacitance would limit the IF bandwidth. To avoid this, buffer amplifiers are incorporated into the active probe, thus, the IF can be increased to 20 MHz. This has the advantage that the probes can be connected directly to the HP8510. Further, the high 20-MHz IF greatly reduces the effect of LO synthesizer close-in phase noise, which was the dominant error contribution in earlier active probe-based systems, where a 10-kHz IF was used [5].

A. Performance of the Active Probe

An important figure of an NWA system is the raw directivity, where the measured reflection of a short is compared to the reflection of a load. If the raw directivity is poor, it is generally

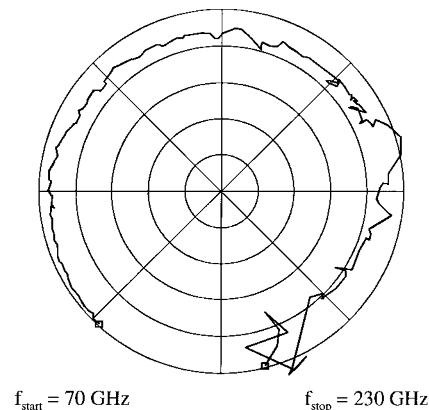

Fig. 17. Measured S_{21} of a 900-μm-long line.

very difficulty to obtain good NWA accuracy after calibration. Fig. 14 shows the result of this measurement. The raw directivity is better than 5 dB, except at a few isolated frequencies and decreases as frequency is increased. The raw directivity is observed to vary with frequency, with a periodicity of approximately 14 GHz, which reflects the length of the flexible micro-coax probe tip. This is indicative of reflections at the IC–tip interface. With an improved connection between the chip and micro-coaxial cable, the directivity can be increased.

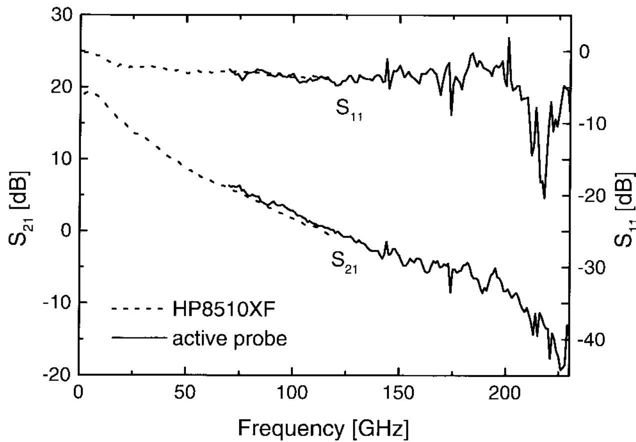

Fig. 18. S_{11} and S_{21} of a pseudomorphic InAlAs/InGaAs HEMT.

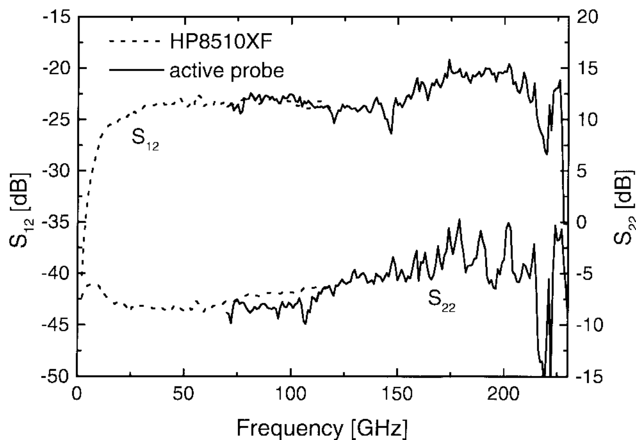

Fig. 19. S_{12} and S_{22} of a pseudomorphic InAlAs/InGaAs HEMT.

Fig. 15 shows the measured maximum power at the IF ports of the active probe including the buffer amplifiers. With −35 dBm up to 200 GHz, enough power is available to use the HP8510 directly. Further, the noise level was measured at the IF ports at −135 dBm/Hz, which reflects the noise of the sampler together with the buffer amplifier.

B. Measurements

The system was calibrated with the thru-reflect-line (TRL) method, where the through standard was a 1-ps thru-line (200 μm), the reflect standard a short circuit, and the line standard a 450-μm-long line. For calibration, the ten-term error model was used [18]. Figs. 16 and 17 show the measurements of a 900-μm-long line. As the reference planes after TRL calibration are in the middle of the through standard, the measured line length is reduced by 100 μm at both ports. Due to the reduced raw directivity of the active probe, the measurement accuracy degrades at the upper end of the bandwidth. With improved packaging, especially that of the connection between the chip and micro-coax probe tip, we should be able to increase the directivity and improve the accuracy.

Fig. 7 shows the measured S-parameters of an integrated coplanar 10-dB directional coupler, designed for 180-GHz center frequency. This coupler is used in the integrated NWA circuit. The couplers were characterized with the active probes (full two-port measurements) and with a broad-band commercial S-parameter setup (HP8510XF). In the overlapping region, from 70 to 120 GHz, the measurements are in good agreement.

Figs. 18 and 19 show S-parameter measurements of an InAlAs/InGaAs HEMT with a pseudomorphic channel, fabricated at our institute [19]. This device attains with a gate length of 0.15 μm, an f_T of 160 GHz, and an $f_{\max}$ of 500 GHz. Over the frequency range where both instruments provide data, the active probe provides transistor S-parameter data in good agreement with the HP8510XF system.

VII. Conclusion

We have demonstrated NLTL-based active probes for on-wafer network analysis. These serve as an S-parameter test set for the HP8510. Accurate S-parameter measurements within the 70–230-GHz range have been demonstrated and compared with measurements from the HP8510XF system up to 120 GHz.

Acknowledgment

The authors gratefully acknowledge B. Agarwal, R. Pullela, D. Mensa, Q. Lee, and J. Guthrie, University of California at Santa Barbara, for their help during IC fabrication, K. Köhler, Institute for Applied Solid State Physics, Freiburg, Germany, for growing the wafers, and H. Walcher and J. Windscheif for their support in chip packaging.

References

[1] P. M. Smith, S.-M. J. Liu, M.-Y. Kao, P. Ho, S. C. Wang, K. H. G. Duh, S. T. Fu, and P. C. Chao, "W-band high efficiency InP-based power HEMT with 600 GHz $f_{\max}$," *IEEE Microwave Guided Wave Lett.*, vol. 5, pp. 230–232, July 1995.

[2] Q. Lee, S. C. Martin, D. Mensa, R. Pullela, R. P. Smith, B. Agarwal, J. Guthrie, and M. Rodwell, "Deep submicron transferred-substrate heterojunction bipolar transistors," presented at the Device Res. Conf., June 1998, Charlottesville, VA.

[3] T. Gaier, M. Barsky, S. Chan, J. Chi, Y. H. Chung, T. W. Huang, P. P. Huang, Y. L. Kok, R. Lai, K. A. Lee, J. Mitchell, M. Nishimoto, L. Samoska, M. Sholley, R. Tsai, H. Wang, and S. Weinreb, "InP HEMT MMIC's for radiometer applications," in *Proc. 2nd ESA Workshop*, May 25–29, 1998, Millilab, Espoo, Finland, pp. 175–180.

[4] R. Lai, M. Barsky, T. Huang, M. Sholley, H. Wang, Y. L. Kok, S. C. Streit, T. Block, P. H. Lui, T. Gaier, and L. Samoska, "An InP HEMT MMIC LNA with 7.2-dB gain at 190 GHz," *IEEE Microwave Guided Wave Lett.*, vol. 8, pp. 393–395, Nov. 1998.

[5] R. Y. Yu, M. Reddy, J. Pusl, S. T. Allen, M. Case, and M. J. W. Rodwell, "Millimeter-wave on-wafer waveform and network measurements using active probes," *IEEE Trans. Microwave Theory Tech.*, vol. 43, pp. 721–729, Apr. 1995.

[6] O. Wohlgemuth, B. Agarwal, R. Pullela, D. Mensa, Q. Lee, J. Guthrie, M. J. W. Rodwell, R. Reuter, J. Braunstein, M. Schlechtweg, T. Krems, and K. Köhler, "A NLTL-based integrated circuit for a 70–200 GHz VNA system," in *Proc. European Microwave Conf.*, vol. 1, 1998, pp. 104–107.

[7] R. Y. Yu, J. Pusl, Y. Konishi, M. Case, M. Kamegawa, and M. J. W. Rodwell, "A time-domain millimeter-wave vector network analyzer," *IEEE Microwave Guided Wave Lett.*, vol. 2, pp. 319–321, Aug. 1992.

[8] M. S. Shakouri, A. Black, B. A. Auld, and D. M. Bloom, "500 GHz GaAs MMIC sampling wafer probe," *Electron. Lett.*, vol. 29, no. 6, pp. 557–558, Mar. 1993.

[9] M. J. W. Rodwell, S. T. Allen, R. Y. Yu, M. G. Case, U. Bhattacharya, M. Reddy, E. Carman, M. Kamegawa, Y. Konishi, J. Pusl, and

R. Pullela, "Active and nonlinear wave propagation devices in ultrafast electronics and optoelectronics," *Proc. IEEE*, vol. 82, pp. 1037–1058, July 1994.

[10] M. J. W. Rodwell, M. Kamegawa, R. Yu, M. Case, E. Carman, and K. S. Giboney, "GaAs nonlinear transmission lines for picosecond pulse generation and millimeter-wave sampling," *IEEE Trans. Microwave Theory Tech.*, vol. 39, pp. 1194–1204, July 1991.

[11] C. J. Madden, R. A. Marsland, M. J. W. Rodwell, D. M. Bloom, and Y. C. Pao, "Hyperabrupt-doped GaAs nonlinear transmission line for picosecond shock-wave generation," *Appl. Phys. Lett.*, vol. 54, no. 11, pp. 1019–1021, Mar. 1989.

[12] U. Bhattacharya, S. T. Allen, and M. J. W. Rodwell, "DC 725-GHz sampling circuits and subpicosecond nonlinear transmission lines using elevated coplanar waveguide," *IEEE Microwave Guided Wave Lett.*, vol. 5, pp. 50–52, Feb. 1995.

[13] C. P. Wen, "Coplanar-waveguide directional couplers," *IEEE Trans. Microwave Theory Tech.*, vol. MTT-18, pp. 318–322, June 1970.

[14] O. Wohlgemuth, T. Krems, R. Reuter, M. J. W. Rodwell, and M. Schlechtweg, "Integrated directional coupler for 90 and 180 GHz," *IEEE Microwave Guided Wave Lett.*, vol. 9, pp. 308–310, Aug. 1999.

[15] W. M. Grove, "Sampling for oscilloscopes and other RF systems: DC through X-band," *IEEE Trans. Microwave Theory Tech.*, vol. 14, pp. 692–635, Dec. 1966.

[16] R. A. Marsland, V. Valdivia, C. J. Madden, M. J. W. Rodwell, and D. M. Bloom, "130 GHz GaAs monolithic integrated circuit sampling head," *Appl. Phys. Lett.*, vol. 55, no. 6, pp. 592–594, Aug. 1989.

[17] R. Y. Yu, M. Case, M. Kamegawa, M. Sundaram, M. J. W. Rodwell, and A. W. Gossard, "275 GHz 3-mask integrated GaAs sampling circuit," *Electron. Lett.*, vol. 26, no. 13, pp. 949–951, June 1990.

[18] D. Rytting, "An analysis of vector measurement accuracy enhancement techniques," presented at the 1992 RF & Microwave Measurement Symp. and Exhibition.

[19] M. Chertouk, M. Dammann, H. Massler, K. Köhler, and G. Weimann, "Passivated 0.15 μm InAlAs/InGaAs HEMT's with 500 GHz $f_{\max}$: HF performance, thermal stability and reliability," presented at the 1998 Int. Symp. Compound Semiconduct., Nara, Japan.

Oliver Wohlgemuth was born in Singen, Germany, in 1968. He received the Dipl.-Ing. degree in electrical engineering from the Technische Hochschule Karlsruhe, Karlsruhe, Germany, in 1996.

In 1996, he joined the Measurement and Characterization Group, Fraunhofer Institute for Applied Solid State Physics, Freiburg, Germany. His research interest are in high-speed electronics, especially nonlinear transmission lines and sampling circuits.

Mr. Wohlgemuth received the 1998 European Microwave Prize.

Mark J. W. Rodwell (M'89) received the B.S. degree from the University of Tennessee, Knoxville, in 1980, and the M.S. and Ph.D. degrees from Stanford University, Stanford, CA, in 1982 and 1988, respectively.

He is currently Professor and Director of the Compound Semiconductor Research Laboratories, University of California at Santa Barbara. From 1982 to 1984, he was with AT&T Bell Laboratories. In 1988, he was a Research Associate at Stanford University. His research explores the limits of high-frequency electronic devices and IC's. Using submicrometer scaling and device modifications, his group developed bipolar transistors with 800-GHz cutoff frequencies, and resonant tunnel diodes with 2-THz cutoff frequencies. His current research focuses on terahertz bipolar transistors, 100-GHz logic, and gigahertz mixed-signal IC's. His group has worked extensively in the area of GaAs Schottky-diode IC's for subpicosecond pulse generation, signal sampling at submillimeter-wave bandwidths, and millimeter-wave instrumentation.

Dr. Rodwell was the recipient of a 1989 National Science Foundation Presidential Young Investigator Award and the 1997 IEEE Microwave Prize.

Ralf Reuter was born in Gelsenkirchen, Germany, on March 17, 1966. He studied electronics, with a main concentration in microelectronics and received the Diplom-Ingenieur and Dr.-Ing. degrees from the Gerhard-Mercator-University, Duisburg, Germany, in 1992 and 1998, respectively.

In 1997, he joined the Fraunhofer Institute for Applied Solid State Physics, Freiburg, Germany, where he is Head of the High Frequency Measurement and Characterization Group. His research interests and activities are in the field of simulation and modeling III–V semiconductor devices. He is also engaged in the investigation of new optimization algorithms based on the theory of evolution for the modeling of electronic devices.

Jürgen Braunstein was born in Essen, Germany, in 1963. He received the Dipl.-Ing. degree and Dr. degree (with honors) from the Technische Hochschule Aachen, Aachen, Germany, in 1989 and 1994, respectively, where he was involved in CMOS and GaInAs MISFET processing technology.

In 1989, he joined the Institute for Applied Solid State Physics, Freiburg, Germany, to investigate reactive ion-etching techniques for GaAs-based MMIC's. From 1990 to 1996, he had been involved in dc and RF characterization of active and passive III/V devices and he had been designing MMIC's for high-speed and power applications. In 1995, he spent seven months at Cornell University as a Visiting Scientist, where he was responsible for high-speed laser and transistor design and characterization. From 1995 to 1996, he managed the RF Characterization Group, Institute for Applied Solid State Physics. The group is specialized in S-parameter measurements up to 200 GHz, noise parameter extraction, large-signal characterization, and the development of new millimeter-wave measurement techniques. Since 1997, he has been heading the Optoelectronic Devices Department, Institute for Applied Solid State Physics, which is predominantly focused on the design, fabrication, and characterization of infrared detectors, including focal plane arrays and semiconductor high-speed and high-power lasers.

Michael Schlechtweg (M'88) was born in Kassel, Germany, in 1958. He received the Dipl.-Ing. degree in electrical engineering from the Technische Hochschule Darmstadt, Darmstadt, Germany, in 1982, and the Dr.-Ing. degree from the University of Kassel, Kassel, Germany, in 1989. His doctoral thesis concerned bias-dependent and nonlinear modeling of MESFET's and MODFET's up to 40 GHz using a table-based large-signal model.

In 1989, he joined the Fraunhofer Institute for Applied Solid State Physics, Freiburg, Germany, where he was involved with the design and characterization of microwave and millimeter-wave IC's. Since 1996, he has been Head of the High Frequency Devices and Circuits Department, Fraunhofer Institute for Applied Solid State Physics. His main research interests are in the areas of high-frequency IC design for communication and sensor systems, and nonlinear characterization of active RF devices.

Dr. Schlechtweg was the recipient of the 1993 Fraunhofer Prize.